PARKINSON'S DISEASE

Commander complex regulates lysosomal function and is implicated in Parkinson's disease risk

Georgia Minakaki†, Nathaniel Safren†, Bernabe I. Bustos, Steven J. Lubbe, Niccolò E. Mencacci, Dimitri Krainc*

Variants in *GBA1* resulting in decreased lysosomal glucocerebrosidase (GCase) activity are a common risk factor for Parkinson's disease (PD) and dementia with Lewy bodies (DLB). Incomplete penetrance of *GBA1* variants suggests that additional genes contribute to PD and DLB manifestation. By using a pooled genome-wide CRISPR interference screen, we identified copper metabolism MURR1 domain–containing 3 (COMMD3) protein, a component of the COMMD/coiled-coil domain–containing protein 22 (CCDC22)/CCDC93 (CCC) and Commander complexes, as a modifier of GCase and lysosomal activity. Loss of COMMD3 increased the release of lysosomal proteins through extracellular vesicles, leading to their impaired delivery to endolysosomes and consequent lysosomal dysfunction. Rare variants in the Commander gene family were associated with increased PD risk. Thus, COMMD genes and related complexes regulate lysosomal homeostasis and may represent modifiers in PD and other neurodegenerative diseases associated with lysosomal dysfunction.

Heterozygous pathogenic variants in *GBA1* represent a common risk factor for the development of Parkinson's disease (PD) and dementia with Lewy bodies (DLB) (*1*–*3*). Carriers of biallelic GBA1 pathogenic variants develop the autosomal recessive lysosomal storage disorder Gaucher disease and are also at risk of developing PD (*4*, *5*). *GBA1* encodes for the lysosomal enzyme glucocerebrosidase (GCase) that hydrolyzes glucosylceramide. Pathogenic *GBA1* variants lead to decreased lysosomal GCase activity, resulting in the accumulation of lipid substrates including glucosylceramide and glucosylsphingosine. Moreover, decreased lysosomal GCase activity has been reported in the absence of *GBA1* pathogenic variants, concomitant with mitochondrial dysfunction and increased α-synuclein levels (*6*, *7*). Pathogenic variants causing a more severe deficit in enzymatic GCase activity are associated with a higher PD risk and earlier age at onset (*4*, *8*). Because the penetrance of pathogenic *GBA1* variants in PD and DLB is incomplete (*9*, *10*), it is likely that additional genetic factors are modifying disease risk in carriers of *GBA1* variants. A genome-wide association study (GWAS) showed that variants nearby the *SNCA* and *CTSB* loci were associated with *GBA1* penetrance in *GBA1*-PD carriers (*11*). Loss of the lysosomal membrane protein TMEM175 reduces GCase activity in cell models, and the *TMEM175* p.Met^{393}Thr variant was associated with reduced GCase activity in human samples from patients with PD (*12*, *13*). Smaller-scale analyses have reported an increased overall burden of rare, likely damaging variants in lysosomal storage disorder–related genes in patients with *GBA1*-PD and PD (*14*, *15*). To gain a better understanding of how specific genes and cellular pathways impact GCase activity and lysosomal homeostasis, we performed a genome-wide pooled CRISPR interference (CRISPRi) screen to identify genetic modifiers of GCase activity and lysosomal function.

[1]Davee Department of Neurology, Northwestern University, Feinberg School of Medicine, Chicago, IL, USA.
*Corresponding author. Email: dkrainc@nm.org
†These authors contributed equally to this work.

A genome-wide CRISPRi screen revealed modulators of lysosomal GCase activity

Lysosomal GCase activity was measured by flow cytometry using 5-(Pentafluorobenzoylamino) Fluorescein Di-β-D-Glucopyranoside (PFB-FDGlu). The intensity of fluorescence emitted upon PFB-FDGlu hydrolysis within the lysosome increased linearly within 10 to 40 min (Fig. 1A). As a positive control, we used CRISPR-Cas9 to knock out *SCARB2*, which encodes for the lysosome integral membrane protein 2 (LIMP-2) that transports GCase to the lysosome (*16*). *SCARB2*–knockout (KO) human embryonic kidney (HEK) cells showed 95% less signal intensity compared with that of isogenic controls (Fig. 1, B and C, and fig. S1A), thus establishing the face validity and sensitivity of the assay. We then performed a genome-wide CRISPRi screen to identify genes modulating lysosomal GCase activity (Fig. 1D). HEK cells stably expressing KRAB-dCas9 were transduced with a genome-scale human CRISPRi version 2 lentiviral library (*17*) (Fig. 1D). Enzymatic activity was assessed 13 days after transduction, and the lowest and highest 30% fluorescence intensity fractions were isolated by fluorescence-activated cell sorting (FACS), followed by sequencing (Fig. 1D). We nominated 338 hit genes as potential modifiers of lysosomal GCase activity using criteria that accounted for both effect size and statistical significance of single guide RNA (sgRNA) enrichment in the low fraction compared with that in the high fraction relative to the distribution of nontargeting sgRNAs (Fig. 1, E and F, and table S1). The 190 low-fraction hits were genes with a knockdown phenotype of reduced activity, whereas the 148 high-fraction hits comprised genes with a knockdown phenotype of increased activity. Both *GBA1* and *SCARB2* were identified as low-fraction hits, thus validating the ability of the screen to appropriately nominate genes. The top two low-fraction hits were copper metabolism MURR1 domain–containing 3 (*COMMD3*) and *COMMD3-BMI1*, the latter representing a transcriptional read-through product resulting from *COMMD3* and its downstream gene on chromosome 10, the transcription repressor *BMI1*. The *COMMD* genes constitute a highly conserved family, with 10 members implicated in nuclear factor κB (NF-κB) signaling and endosomal sorting (*18*–*20*). Additional low-fraction genes included *COMMD9*, encoding for a second COMMD family member, as well as *RAB7A* and the Homotypic fusion and protein sorting (HOPS) complex subunits *VPS16*, *VPS39*, and *VPS41* (Fig. 1F). *REL* and insulin-like growth factor 1 receptor (*IGF1R*) were amongst the top 10 high-fraction hits (Fig. 1F).

We conducted a secondary small interfering RNA (siRNA) screen for a subset of 37 nominated hit genes, including *GBA* and *SCARB2*, as positive controls. Knockdown was confirmed for *SCARB2* and *VPS16*, showing an 80 and 60% reduction in the encoded proteins LIMP-2 and VPS16, respectively (fig. S1, B and C). *GBA1* knockdown for 48 hours reduced activity by 30%, whereas *SCARB2* knockdown resulted in 50% lower activity. Furthermore, siRNA against *RAB7A*, *VPS16*, *VPS39*, and *VPS41* reduced enzymatic activity by 30 to 60% (fig. S1D). To further investigate the role of VPS16 deficiency in GCase homeostasis, we used fibroblasts from a patient carrying a heterozygous pathogenic *VPS16* variant in exon 18 (c.1813C>T, NM_022575.4). Relative to two control lines, this line had a 50% reduction in VPS16 protein and a 40% reduction in GCase activity, an effect that could not be attributed to impaired substrate uptake through endocytosis (pinocytosis), as assessed by dextran uptake (fig. S1, E to G). Collectively, the data validate HOPS complex–related genes as lysosomal GCase activity modifiers. It is possible that some of the hits not validated by siRNA represent false negatives due to inefficient knockdown during two days of silencing.

We further investigated *IGF1R* and *REL*, genes with a CRISPRi phenotype of increasing lysosomal GCase activity. After 24 hours of treatment with the dual IGF1R and insulin receptor (IR) inhibitor, Linsitinib (OSI-906), as well as the c-REL inhibitor, IT-603, lysosomal GCase activity in HEK cells was increased by 50% without affecting substrate uptake (fig. S2A). IT-603 also

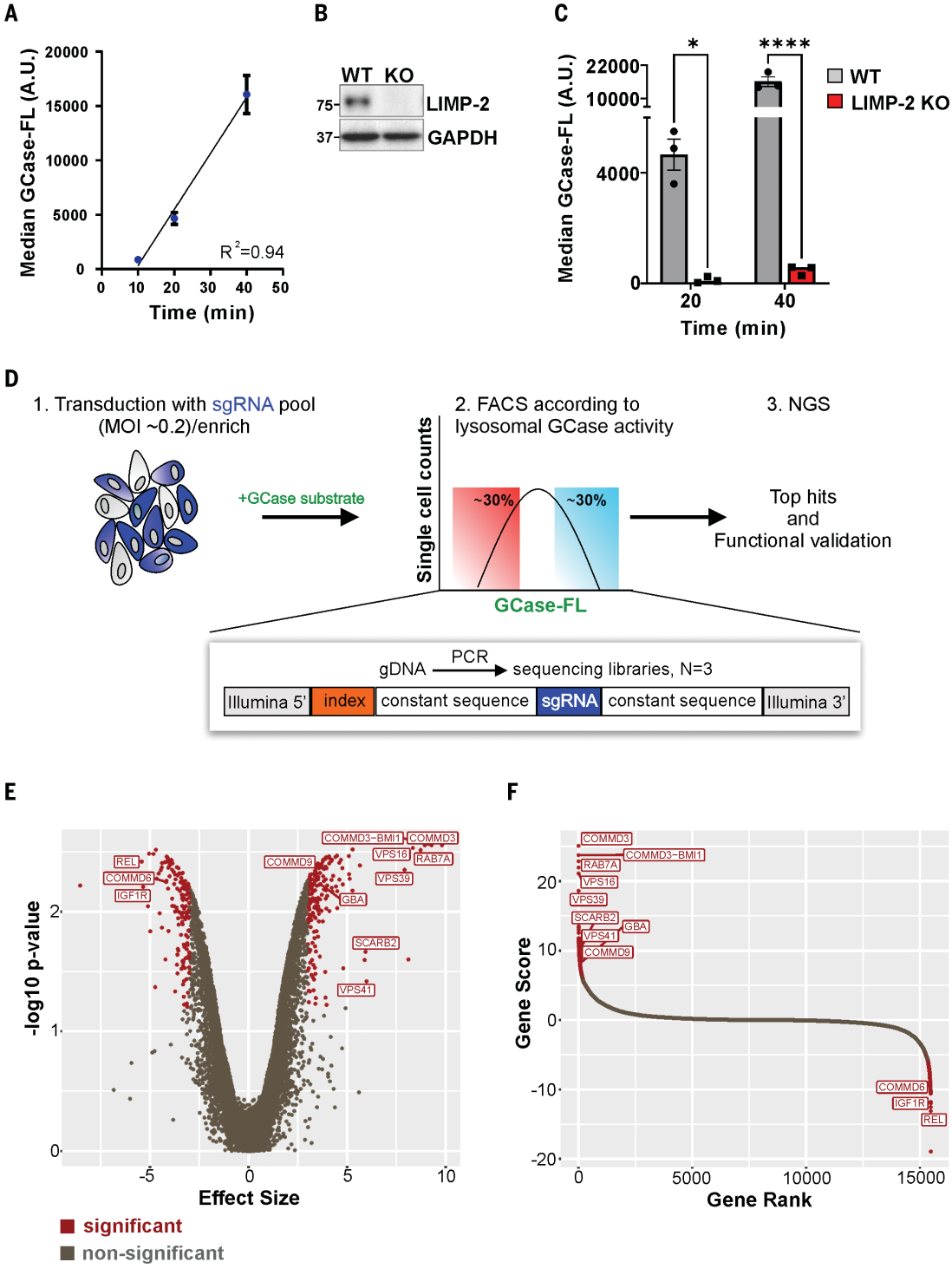

Fig. 1. Identification of candidate modifiers of lysosomal GCase activity through a genome-wide CRISPRi screen. (**A**) Flow cytometry of fluorescence intensity (A.U., arbitrary units), representing lysosomal GCase activity, upon incubation with the substrate PFB-FDGlu for the indicated times (750 μM; 100,000 single cells recorded). Data represent mean ± SEM; $N = 3$ independent experiments. FL, fluorescence. (**B**) Western blot analysis of LIMP-2 protein in WT or CRISPR-Cas9 *SCARB2*-KO HEK cells with GAPDH used as a loading control. GAPDH, glyceraldehyde-3-phosphate dehydrogenase. (**C**) Flow cytometry assessment of lysosomal GCase activity in HEK cells. Data represent mean ± SEM; $N = 3$ independent experiments. Two-way analysis of variance (ANOVA) with Šídák's post hoc test: $F_{genotype(1,\ 8)} = 118.8$, $P < 0.0001$; $^{*}P < 0.05$; $^{****}P < 0.0001$. (**D**) Workflow of the CRISPRi screen, performed $N = 3$ independent experiments in dCas9-KRAB HEK-293 cells. gDNA, genomic DNA; PCR, polymerase chain reaction; MOI, multiplicity of infection; NGS, next-generation sequencing. (**E**) Volcano plot shows genes and pseudogenes identified in the FACS fractions, with red dots representing nominated hits according to statistical significance and a z score >3. Red genes were selected for functional validation. (**F**) Genes ordered by gene score (z score × $-\log_{10}P$ value), with red dots indicating significant hits.

increased GCase activity by 25% in induced pluripotent stem cell (iPSC)–derived forebrain neurons (iNeurons) from an individual with PD carrying *GBA1* p.N409S+/− (fig. S2B).

Loss of COMMD3 reduced lysosomal GCase activity in iPSC-derived microglia and neurons

The top low-fraction hit gene *COMMD3* is part of a 12-protein complex consisting of COMMD1 to COMMD10, coiled-coil domain–containing protein 22 (CCDC22), and CCDC93; thus, it is named the CCC complex (*21*–*23*). The Commander complex is formed through functional interaction of CCC with DENND10 and Retriever and, together with the WASH complex, participates in retromer-independent endosomal recycling (*21*–*24*). Two independent HEK COMMD3-KO clones showed 50 to 60% lower lysosomal GCase activity, independent of substrate uptake (Fig. 2, A and B). In addition, we knocked out COMMD3 in a control iPSC line and differentiated these cells to microglia (iMGs) and iNeurons (*25*, *26*). COMMD3 deficiency lowered lysosomal GCase activity in both cell types (Fig. 2, C and D). To address whether reintroducing COMMD3 would be sufficient to rescue lysosomal GCase activity in COMMD3-KO cells, we generated HEK cell lines stably expressing COMMD3–red fluorescent

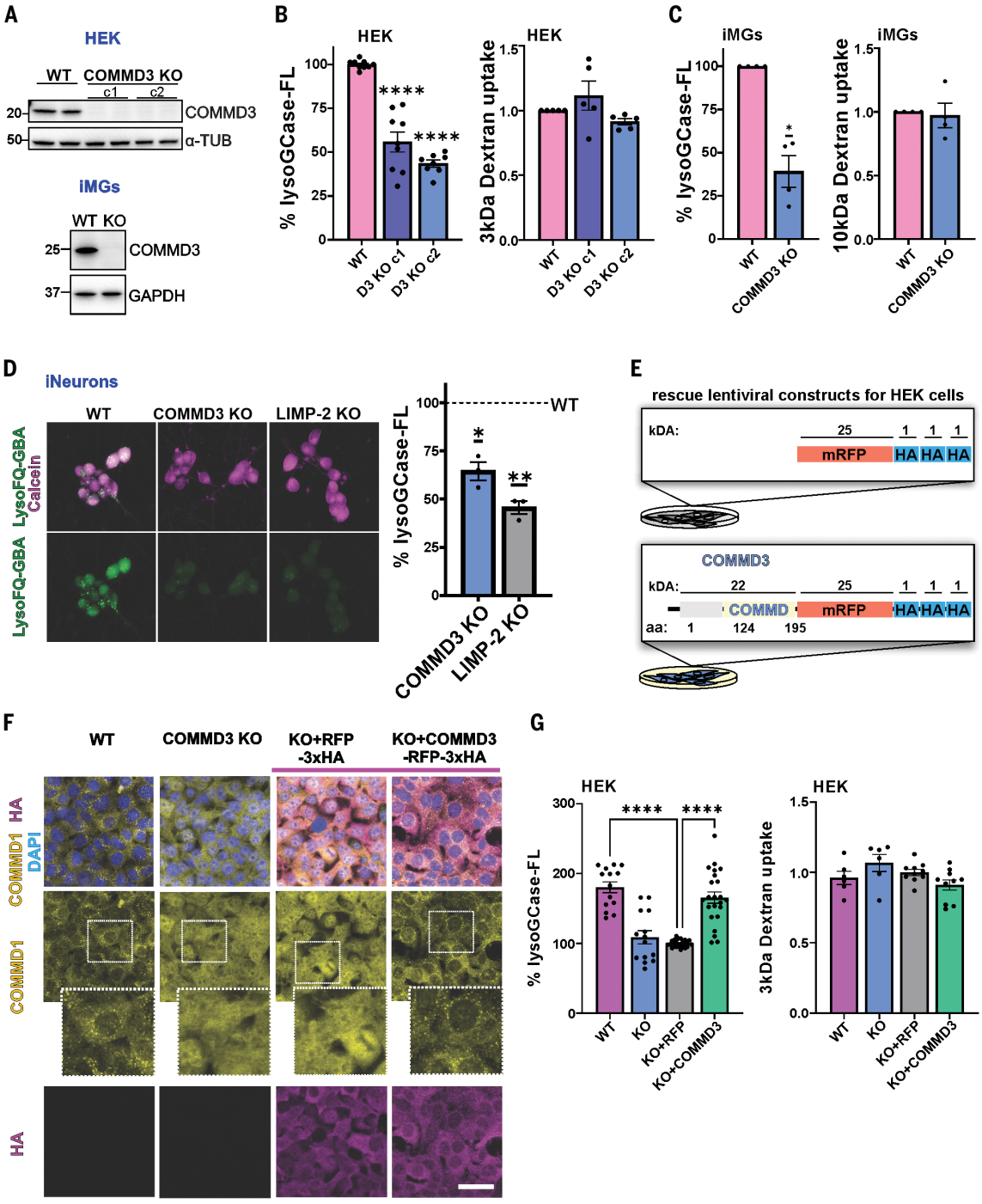

Fig. 2. COMMD3 knockout reduced lysosomal GCase activity. (**A**) Western blot analysis of COMMD3 protein in two clones (c1 and c2) of CRISPR-Cas9 COMMD3-KO HEK cells and one clone of iMGs. α-tubulin (α-TUB) or GAPDH were the loading controls. (**B**) Flow cytometry examination of lysosomal GCase activity (250-μM PFB-FDGlu for 30 min; 20,000 single cells recorded) and dextran uptake in HEK cells (200-μg/mL 3-kDa dextran for 30 min). Data represent mean ± SEM; $N = 5$ independent experiments. One-way ANOVA with Dunnett's post hoc test: $F_{lysoGCase(2,23)} = 68.81$, $P < 0.0001$; $F_{dextran\ uptake(2,12)} = 2.326$, $P = 0.14$; ****$P < 0.0001$. (**C**) Flow cytometry of lysosomal GCase activity (188-μM PFB-FDGlu for 20 min; 10,000 to 20,000 single cells recorded) or dextran uptake (100-μg/mL 10-kDa dextran) in iMGs. Data represent mean ± SEM; $N = 4$ independent experiments. One-sample t test; *$P = 0.025$. (**D**) Automated imaging analysis of lysosomal GCase activity (LysoFQ-GBA fluorescence, green) in iNeurons labeled with calcein (magenta). Data represent mean ± SEM; $N = 3$ independent experiments. One-sample t test; *$P = 0.0173$; **$P = 0.0037$. (**E**) Lentiviral constructs used to generate stable HEK cell rescue lines. (**F**) Immunocytochemistry examination of COMMD1 puncta (deep yellow), reflecting CCC and Commander complex formation, in HEK cells under baseline or upon transduction with the indicated HA-tagged constructs (magenta). (**G**) (Left) Flow cytometry of lysosomal GCase activity (250-μM PFB-FDGlu for 30 min; 20,000 to 50,000 single cells recorded) in HEK cells. Data represent mean ± SEM; WT and KO, $N = 6$; KO + RFP and KO + COMMD3, $N = 9$ independent experiments. One-way ANOVA with Dunnett's post hoc test: $F_{lysoGCase(3,\ 70)} = 33.53$, $P < 0.0001$; ****$P < 0.0001$. (Right) Flow cytometry of dextran uptake (200-μg/mL 3-kDa dextran). Data represent mean ± SEM; WT and KO, $N = 3$ independent experiments; KO + RFP and KO + COMMD3, $N = 5$ independent experiments. One-way ANOVA: $F_{dextran\ uptake(3,\ 28)} = 2.720$, $P = 0.0633$.

protein (RFP)–3×hemagglutinin (HA) or RFP-3×HA as a control (Fig. 2E). We validated that the exogenous COMMD3-RFP-3×HA puncta colocalized with endogenous COMMD1, confirming that exogenous COMMD3 could functionally interact with CCC and Commander complex constituents (fig. S2C). COMMD3 knockout abolished the formation of COMMD1 puncta and led to the cellular depletion of CCDC22 in HEK cells and iNeurons (Fig. 2F and fig. S2, D and E). However, *COMMD1* and *CCDC22* expression was not affected in COMMD3-KO HEK cells (fig. S2D), suggesting that the encoded proteins were unstable in the cytoplasm. These findings are in accordance with previous reports that knockout of individual COMMD proteins can disrupt Commander complex formation (*27*). In COMMD3-KO cells stably expressing COMMD3-RFP-3×HA, COMMD1 puncta formation, CCDC22 expression, and GCase activity were restored (Fig. 2, F and G, and fig. S2D). Because COMMD3 add-back was sufficient to restore GCase activity in COMMD3-KO cells, it is very unlikely that the decrease in enzymatic activity observed upon *COMMD3-BMI1* CRISPRi was mediated by BMI1.

Deficiency of COMMD3 impaired the delivery of lysosomal proteins leading to lysosomal dysfunction

To investigate the mechanism by which COMMD3 knockout reduces lysosomal GCase activity, we examined the abundance of lysosomal proteins (fig. S3, A and B). In total cell lysates from COMMD3-KO and wild-type (WT) HEK cells, no differences were found in the amounts of GCase, LIMP-2, hexosaminidase B (HEXB), or lysosome-associated membrane protein 2 (LAMP2), nor in the amounts of prosaposin, progranulin, and cathepsin B, which have been reported to modulate GCase activity (*28*–*30*) (fig. S3, A and B). By using transmission electron microscopy, we observed similar amounts of individual organelles in WT and COMMD3-KO cells (fig. S4A), and automated image analysis showed comparable LAMP1 puncta per cytoplasmic area (fig. S4B). Similarly, GCase and LIMP-2 amounts were not altered in total lysate from COMMD3-KO iPSC-derived dopaminergic (DAergic) neurons (fig. S3C), and gene expression of *GBA1* and *SCARB2* was not altered either (fig. S5, A and B). We also did not detect an enrichment of differentially expressed genes in the transcription factor EB transcriptional network (fig. S5C).

Although total cell lysates did not reveal major changes in endolysosomal protein abundance, lysosomal degradation efficiency, assessed by the DQ bovine serum albumin (BSA) assay, was reduced in COMMD3-KO cells in the absence of alterations in lysosomal acidity (Fig. 3A). To examine the mechanisms mediating decreased lysosomal degradation capacity, endolysosomes were immunopurified (Lyso-IP) by generating HEK lines stably expressing LAMP1-RFP-3×HA (*31*, *32*). COMMD3-KO endolysosomes from two independent clones showed 30 to 40% reduction in LAMP2 protein, 40% lower LIMP-2, 30 to 40% lower GCase amounts, and 30 to 40% reduced cathepsin B compared with WT endolysosomes (Fig. 3, B and C). Levels of GCase, LIMP-2, and cathepsin B were also decreased in endolysosomes purified from COMMD3-KO iPSC-derived DAergic neurons (Fig. 3D), suggesting that COMMD3 depletion impedes the delivery of LIMP-2 and GCase to the endolysosomal compartment.

Furthermore, COMMD3-KO endolysosomes had 2.7-fold-higher prosaposin than WT endolysosomes (fig. S6, A and B). By using an antibody specific for saposin C (fig. S6C), a prosaposin fragment that is an endogenous GCase activator (*28*, *29*), we found that the fraction of saposin C to full-length prosaposin was 60% reduced in COMMD3-KO endolysosomes (Fig. 3E), suggesting deficient cleavage. We extended the analysis to progranulin, which interacts with prosaposin and is reported to modulate GCase activity through its cleavage products granulins (*30*, *33*–*35*). Similarly to prosaposin, we found three-fold-higher full-length progranulin amounts in COMMD3-deficient cells (fig. S6D) and a 70% decrease in the ratio of a 7-kDa fragment (*36*, *37*) to full-length progranulin, thus revealing deficient progranulin processing (fig. S6, D and E). These data suggest that CCC and Commander complex deficiency can reduce GCase activity owing to defective processing of prosaposin and progranulin, which is expected to have a broader impact on lysosomal homeostasis.

Lysosomal proteins are released through extracellular vesicles upon loss of COMMD3

Considering the role of CCC and Commander complexes in endosomal recycling, we investigated whether COMMD3 deficiency may impact the cotrafficking of LIMP-2 and GCase through endosomes with the retention using selective hooks (RUSH) assay (*38*, *39*). mCherry-LIMP-2 and enhanced green fluorescent protein (eGFP)–GCase were fused to streptavidin binding protein (SBP) and retained in the endoplasmic reticulum (ER) owing to coexpression of a Streptavidin-KDEL fragment (Fig. 4, A and B). Upon addition of biotin, exogenous LIMP-2 and GCase moved through the ER and Golgi with similar kinetics in WT and COMMD3-KO HEK cells (Fig. 4C). However, upon exiting the Golgi at 45 to 60 min, LIMP-2 and GCase accumulated in post-Golgi vesicles in COMMD3-KO cells, some of which were positive for the early endosome marker EEA1 (Fig. 4C). The phenotype of LIMP-2$^+$/GCase$^+$/EEA1$^+$ vesicle accumulation was most prominent at 1.5 to 2 hours after biotin treatment (Fig. 4, C and D). We hypothesized that protein retention in early endosomes may promote their internalization into intralumenal vesicles within late endosomes (multivesicular bodies) and their subsequent release in association with exosomes/extracellular vesicles (EVs) (*40*). Examination of EV fractions isolated by ultracentrifugation from conditioned medium showed that LAMP1 and LIMP-2 were prominently detected in COMMD3-KO EVs, whereas they were marginally detectable in WT and COMMD3 rescue fractions (Fig. 4, E and F, and fig. S6F). The association of LIMP-2 with COMMD3-KO EVs was further validated by using magnetic CD9/63/81$^+$ EV immunoisolation (fig. S6F). Moreover, HEXB was increased fourfold in COMMD3-KO EVs compared with those of WT and COMMD3 rescue lines (fig. S6G). All fractions were positive for the EV markers flotillin-1 (FLOT1) and ALG-2–interacting protein X (ALIX), with FLOT1 increased by 2.4-fold in COMMD3-KO EVs, whereas ALIX abundance was similar amongst the EV fractions (Fig. 4, E and F, and fig. S6G). Furthermore, COMMD3-KO EVs from d90 iPSC-derived DAergic neurons exhibited 12-fold-higher LAMP1 and threefold-higher HEXB protein (Fig. 4F). These data suggest that loss of COMMD3 promotes the release of certain lysosomal proteins in lieu of their lysosomal delivery, partly because of their increased retention in the early endocytic compartment (fig. S9).

Loss of COMMD9 reduced lysosomal GCase activity in iPSC-derived neurons

COMMD9 represents the second top hit gene of the COMMD protein family (Fig. 1, E and F). To determine the effects of COMMD9 loss, COMMD9-KO iPSCs were generated and differentiated into iNeurons. MAP2 and TUJ1 staining demonstrated that differentiation into iNeurons was not impacted by COMMD3 or COMMD9 knockout (fig. S5D). Loss of COMMD9 reduced COMMD1 and CCDC22 amounts (fig. S7A), as expected (*27*), and led to lower lysosomal GCase activity (fig. S7B), thus validating COMMD9 as a GCase activity modifier.

Increased burden of loss-of-function variants in CCC and Commander complex genes in PD

To explore whether CCC and Commander complex dysfunction may be linked to increased PD risk, we performed a case-control gene set burden analysis of predicted rare loss-of-function variants (LOF, frequency < 1%) in three gene sets: (i) the COMMD ring (10 genes), (ii) the CCC complex (13 genes), and (iii) the Commander complex (17 genes) (see materials and methods). By using the CMC-Wald test and a fixed-effect meta-analysis between two analyzed PD cohorts (the AMP-PD whole-genome sequencing cohort and the UK Biobank whole-exome cohort, totaling 6166 PD cases and 109,467 controls), we found an increased burden of rare coding LOF variants in the COMMD ring [meta-analysis $P = 1.79 \times 10^{-5}$, odds ratio (OR) = 2.43,

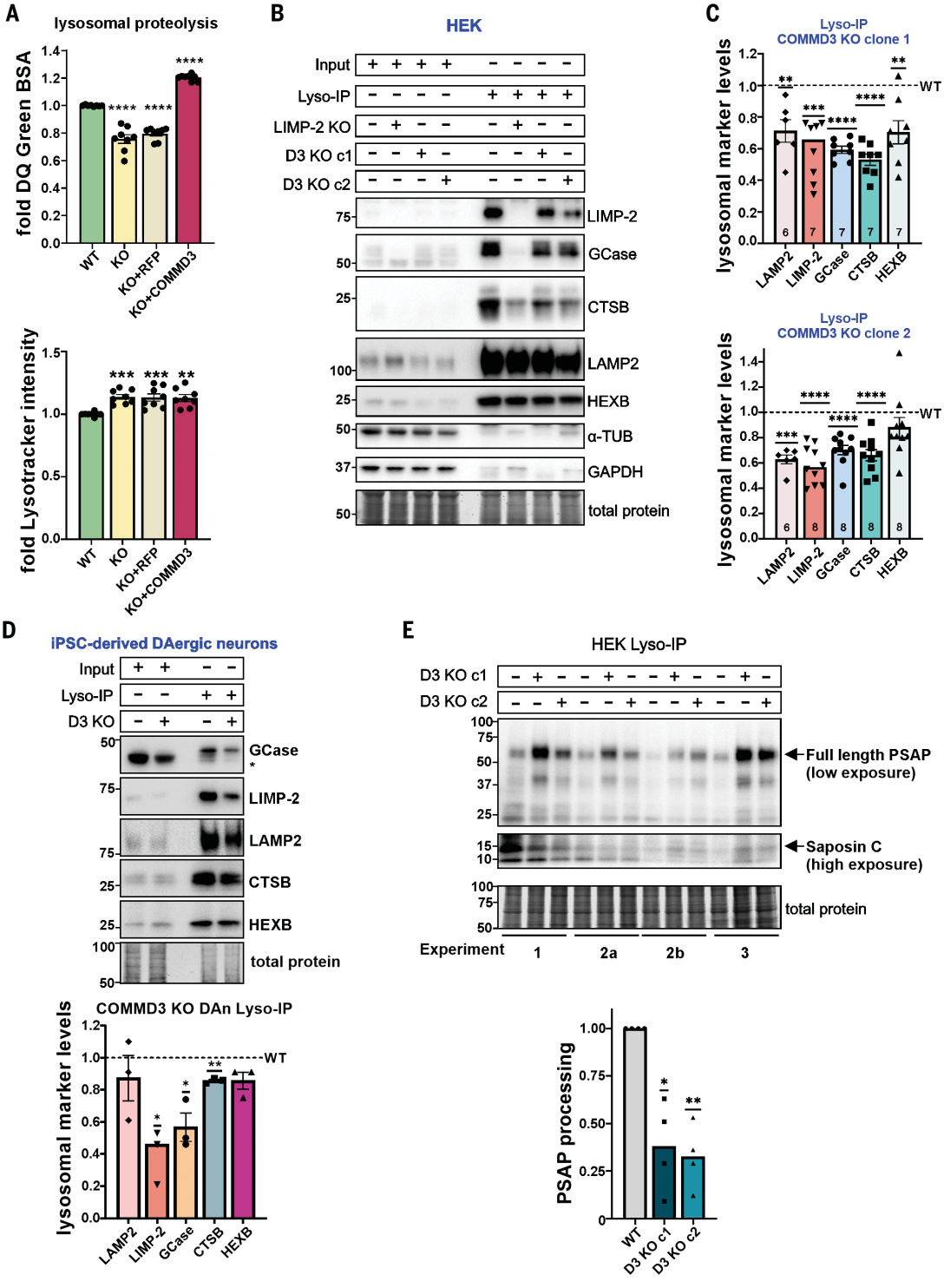

Fig. 3. Loss of COMMD3 function led to lysosomal dysfunction. (**A**) Flow cytometry assessment of lysosomal proteolysis (25-μg/mL DQ Green BSA for 5 hours; 50,000 single cells recorded). Data represent mean ± SEM; *N* = 4 independent experiments. Flow cytometry assessment of endolysosomal acidity (100-nM Lysotracker Green for 30 min; 50,000 single cells). Data represent mean ± SEM; *N* = 4 independent experiments. One-way ANOVA with Dunnett's post hoc test: $F_{proteolysis(3,28)}$ = 127.8, *P* < 0.0001; $F_{Lysotracker(3,28)}$ = 8.919, *P* = 0.0003. ***P* = 0.001; ****P* < 0.0008; *****P* < 0.0001. (**B**) Western blot examination of Lyso-IP fractions from cells expressing LAMP1-RFP-3×HA. (**C**) Protein amounts were normalized to total loaded protein (SimplyBlue stain on electrophoresis gel) and expressed over WT control, indicated by dashed line. Data represent mean ± SEM, *N* = 6 to 8 independent experiments. One-sample *t* test; ***P* = 0.001; ****P* ≤ 0.0007. (**D**) Western blot analysis of Lyso-IP from d104 iPSC-derived DAergic neurons (DAns). Protein amounts were normalized to total loaded protein (SimplyBlue stain on electrophoresis gel) and expressed over WT control, indicated by dashed line. Data represent mean ± SEM; *N* = 3 independent experiments. One-sample *t* test; **P* < 0.05; ***P* = 0.0038. (**E**) Western blot analysis of prosaposin (PSAP) in Lyso-IP fractions using an antibody specific for both the full-length and 15-kDa saposin C fragment (specificity shown in fig. S6C). Protein amounts were normalized to total loaded protein (SimplyBlue). The graph shows saposin C to full-length PSAP ratio, expressed as fold change over WT control. Data represent mean ± SEM; *N* = 4 independent experiments. One-sample *t* test; **P* = 0.014; ***P* = 0.0042.

95% confidence interval (CI) =1.62 to 3.64], the CCC complex (meta-analysis $P = 4.87 \times 10^{-7}$, OR = 2.56, 95% CI = 1.78 to 3.70), and the Commander complex (meta-analysis $P = 1.79 \times 10^{-5}$, OR = 2.13, 95% CI = 1.53 to 2.96) (Fig. 5 and table S2). We also investigated burden of rare variants in gene sets, including the Retriever complex (three genes) and the HOPS complex (six genes), and found no evidence of enrichment in cases versus controls (Fig. 5 and table S2).

When individual gene burden was assessed, *COMMD9* showed significance in the UK Biobank cohort [false discovery rate (FDR)–adjusted $P = 2.24 \times 10^{-2}$, OR = 6.10, 95% CI = 2.07 to 17.94] and the same direction of the effect in the AMP-PD cohort (FDR-adjusted *P* = 0.96, OR = 2.17, 95% CI = 0.04 to 108.79) (table S3). However, a larger sample size will be required to

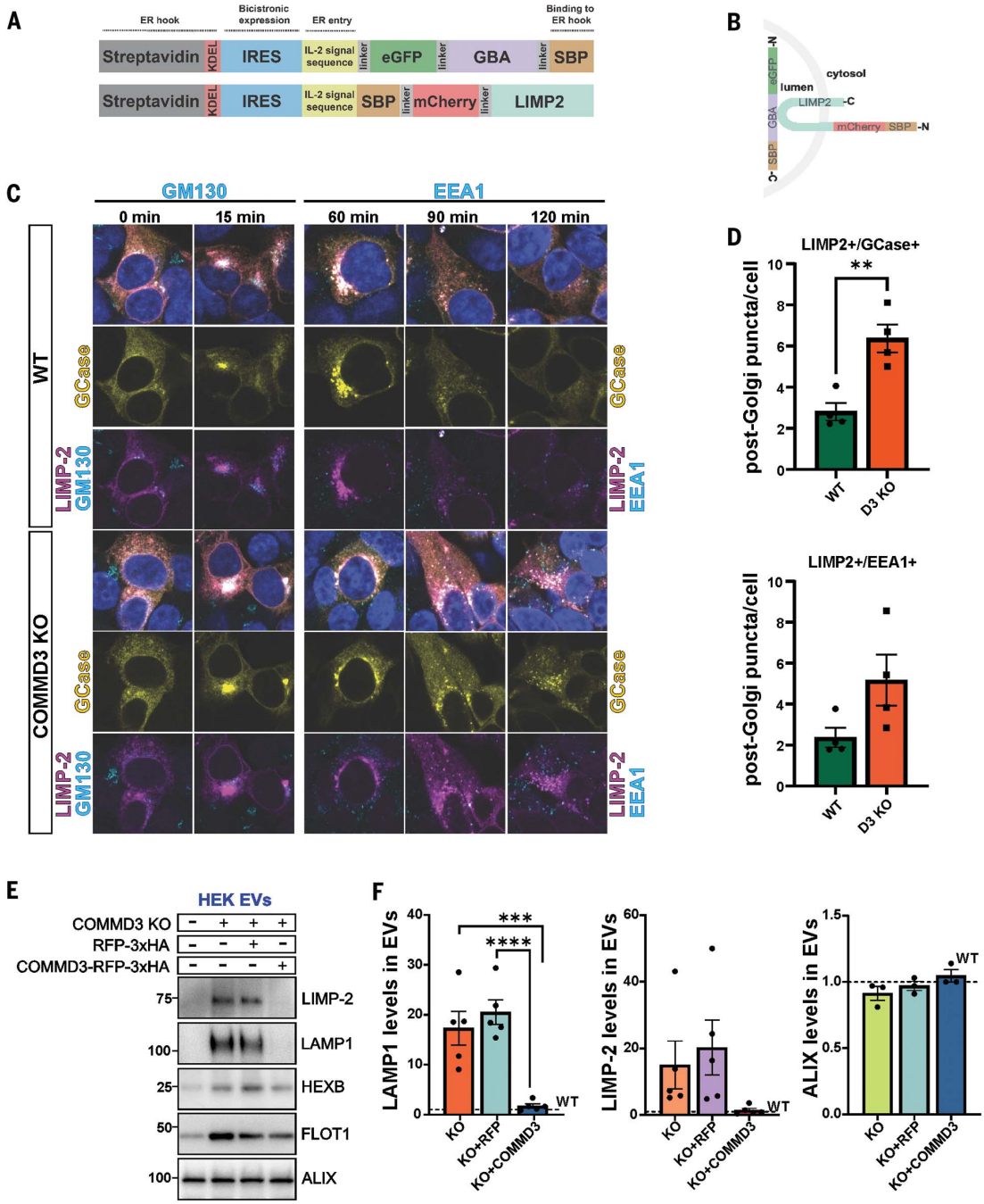

Fig. 4. Lysosomal proteins were retained in post-Golgi vesicles and released through EVs upon loss of COMMD3. (**A**) Schematic representation of GBA and LIMP-2 RUSH constructs. IRES, internal ribosome entry site. (**B**) Illustration depicting orientation of RUSH-synchronized GCase and LIMP2 following biotin addition and ER exit. (**C**) Immunofluorescence images of eGFP-GBA-SBP (deep yellow) and SBP-mCherry-LIMP2 (magenta) at the indicated time points following treatment with 40-μM biotin. GM130 (cyan) was used as a Golgi marker in 0- and 15-min panels, and EEA1 (cyan), as an early endosome marker in 60-, 90-, and 120-min panels. Scale bar, 10 μm. (**D**) Quantification of the number of colocalized SBP-mCherry-LIMP2 and eGFP-GBA-SBP puncta per cell 90 min after biotin addition. Each dot represents the mean number of puncta in an experimental replicate. Data represent mean ± SEM; $N = 4$ independent experiments. Two-sample t test; $^{**}LIMP2^{+}/GCase^{+}$ $P = 0.0043$. (**E**) Western blot of the EV fraction obtained from identical volumes of 24-hour conditioned medium. (**F**) Graphs show mean ± SEM protein amounts over WT, indicated by the dashed line; $N = 3$ to 6 independent experiments. One-way ANOVA with Tukey's post hoc test: $F_{LAMP1(3,16)} = 23.70$, $P < 0.0001$; $F_{LIMP\text{-}2(3,16)} = 3.157$, $P = 0.0537$; $F_{ALIX(3,8)} = 2.062$, $P = 0.1838$. $^{***}P = 0.0004$; $^{****}P < 0.0001$.

validate this association. Detailed annotation and allele count in cases and controls for the variants included in all analyzed genes are provided in table S4. Collectively, these results show that there is a substantial burden of rare LOF variants in the Commander complex and its constituent CCC complex and COMMD ring that contribute to risk of PD in two independent case-control populations.

Expression of Commander complex proteins in forebrain of PD or DLB patients

To address whether Commander complex constituents are altered in patient brains, we examined forebrain samples from seven DLB cases and seven controls (fig. S8, A and B). The amount of COMMD3, COMMD1, and CCDC22 protein was reduced in DLB samples relative to controls (fig. S8B). However, owing to variability within the groups, the assessment of a larger number of samples will be important for understanding the potential contribution of WT CCC and Commander complex deficit in PD, DLB, and other neurodegenerative diseases.

Discussion

The Commander complex consists of a heteropentameric ring of COMMD protein dimers, whose stable association with the Retriever complex is mediated by extensive interactions with CCDC22 and CCDC93 (*24*, *41*, *42*). Each COMMD preferentially heterodimerizes with one other COMMD protein, and the loss of one component can potentially destabilize the entire Commander complex (*24*, *27*, *41*–*46*). Consistent with this notion, COMMD3 loss disrupted complex formation, which was restored by exogenous COMMD3. The CCC and Commander complexes are indispensable for recycling of Retriever cargo from endosomes to the plasma membrane (*43*, *45*, *47*, *48*), and our data reveal their expanded role in lysosomal function. We

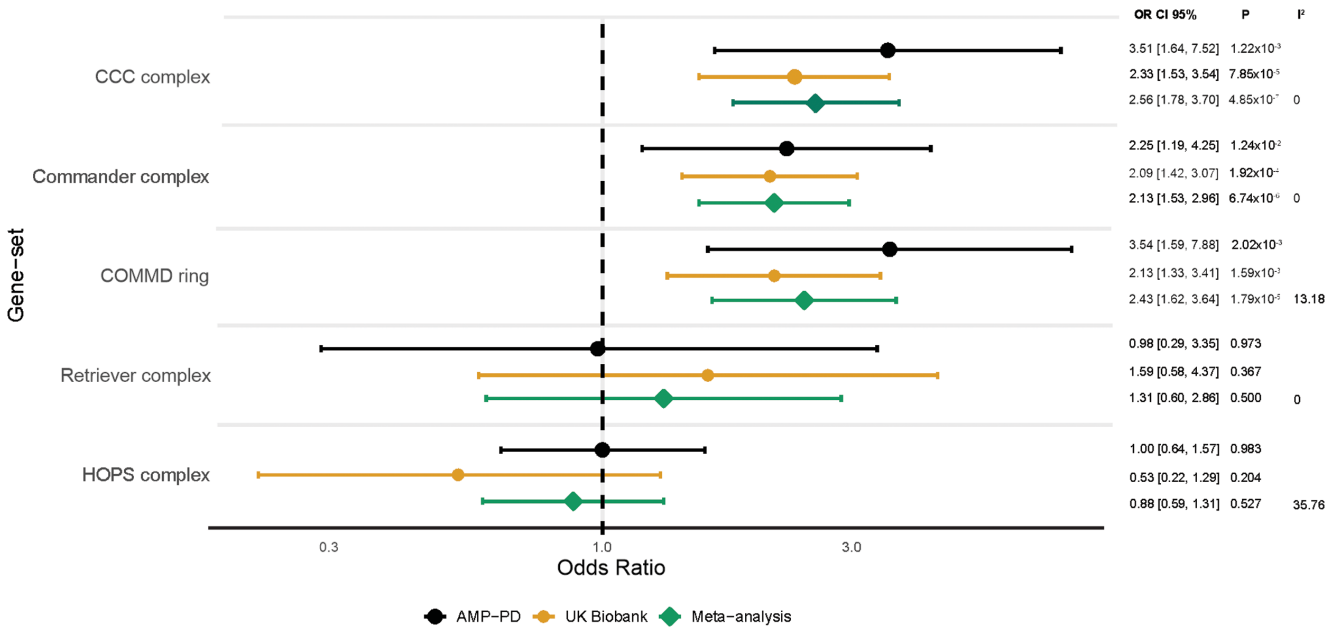

Fig. 5. Increased burden of LOF variants in COMMD-related genes in PD. Forest plots showing study-wise and fixed-effects meta-analysis ORs and *P* values from the burden of rare coding LOF variants for CCC complex, Commander complex, COMMD ring, Retriever, and HOPS complex gene sets. Horizontal bars represent 95% confidence intervals of the ORs, and I^2 is the percentage of meta-analysis heterogeneity.

found that COMMD3 loss resulted in partial retention of lysosomal proteins in endosomes, followed by their release through EVs in lieu of lysosomal delivery, ultimately leading to lysosomal dysfunction.

Disruption of the Commander complex decreased GCase activity partly due to reduced amounts of the enzyme and its transporter LIMP-2 within lysosomes paralleled by GCase or LIMP-2 retention in early endosomes. Furthermore, loss of Commander function reduced GCase activity through deficient prosaposin processing to the endogenous GCase activator saposin C and progranulin to granulin fragments. Impaired progranulin processing can also impact cathepsin D activity (*30*, *49*–*51*) and general lysosomal homeostasis through its stabilizing interaction with bis(monoacylglycero)phosphate (BMP), a lipid cofactor in lysosomal proteolysis and lipolysis (*52*–*54*). Because cathepsin B mediates prosaposin and progranulin processing (*28*, *37*), deficient prosaposin or progranulin processing may be partly attributed to the reduced amount of mature cathepsin B upon COMMD3 loss of function. A variant proximal to the *CTSB* locus, expected to increase cathepsin B amounts, was associated with decreased PD risk in *GBA1* carriers (*11*). Therefore, decreased amounts of cathepsin B owing to Commander complex deficiency may represent an intriguing converging pathway that modulates GCase activity and contributes to PD risk.

A subset of our high-fraction CRISPRi hit genes encode for druggable proteins and may therefore inform future efforts to enhance lysosomal GCase activity through small-molecule drugs. As a proof of concept, we demonstrated that inhibition of *REL* with IT-603 increased lysosomal GCase activity. Nevertheless, the protein product of *REL*, c-Rel, is an NF-κB subunit whose diverse roles in inflammation, B cell proliferation, and cancer need careful consideration when evaluating its translational potential (*55*).

We found an association of rare variants in the COMMD gene family with increased risk for PD. Although no common or rare variants in COMMD genes have been previously associated with PD risk (*56*–*58*), our detection of the association was enabled by the genome-wide CRISPRi screen and subsequent validation. The low frequency of predicted COMMD LOF variants in the population may be due to the key role that these genes play in trafficking of hundreds of plasma membrane proteins. For example, COMMD9 knockout is embryonic lethal in mice owing to cardiac abnormalities due to deficient Notch2 trafficking (*48*).

Our findings suggest that CCC and Commander complex deficiency impacts lysosomal homeostasis and that *COMMD* variants may represent disease risk modifier genes in PD, DLB, and potentially other neurodegenerative diseases that exhibit lysosomal dysfunction. It will be of interest to examine whether therapeutic targeting of the COMMD pathway may improve lysosomal function in these disorders.

REFERENCES AND NOTES

1. R. Chia *et al.*, *Nat. Genet.* **53**, 294–303 (2021).
2. E. Sidransky *et al.*, *N. Engl. J. Med.* **361**, 1651–1661 (2009).
3. D. Tsuang *et al.*, *Neurology* **79**, 1944–1950 (2012).
4. R. N. Alcalay *et al.*, *JAMA Neurol.* **71**, 752–757 (2014).
5. B. Rosenbloom *et al.*, *Blood Cells Mol. Dis.* **46**, 95–102 (2011).
6. L. F. Burbulla *et al.*, *Science* **357**, 1255–1261 (2017).
7. J. R. Mazzulli *et al.*, *Cell* **146**, 37–52 (2011).
8. Z. Gan-Or *et al.*, *Neurology* **84**, 880–887 (2015).
9. M. Anheim *et al.*, *Neurology* **78**, 417–420 (2012).
10. R. Balestrino *et al.*, *Mov. Disord.* **35**, 2111–2114 (2020).
11. C. Blauwendraat *et al.*, *Brain* **143**, 234–248 (2020).
12. S. Jinn *et al.*, *Proc. Natl. Acad. Sci. U.S.A.* **114**, 2389–2394 (2017).
13. L. Krohn *et al.*, *Ann. Neurol.* **87**, 139–153 (2020).
14. L. A. Robak *et al.*, *Brain* **140**, 3191–3203 (2017).
15. L. Straniero *et al.*, *Mov. Disord.* **37**, 1202–1210 (2022).
16. D. Reczek *et al.*, *Cell* **131**, 770–783 (2007).
17. M. A. Horlbeck *et al.*, *eLife* **5**, e19760 (2016).
18. E. Burstein *et al.*, *J. Biol. Chem.* **280**, 22222–22232 (2005).
19. A. L. Mallam, E. M. Marcotte, *Cell Syst.* **4**, 483–494 (2017).
20. C. Wan *et al.*, *Nature* **525**, 339–344 (2015).
21. P. Bartuzi *et al.*, *Nat. Commun.* **7**, 10961 (2016).
22. K. E. McNally *et al.*, *Nat. Cell Biol.* **19**, 1214–1225 (2017).
23. C. A. Phillips-Krawczak *et al.*, *Mol. Biol. Cell* **26**, 91–103 (2015).
24. M. D. Healy *et al.*, *Cell* **186**, 2219–2237.e29 (2023).
25. M. S. Fernandopulle *et al.*, *Curr. Protoc. Cell Biol.* **79**, e51 (2018).
26. Y. Zhang *et al.*, *Neuron* **78**, 785–798 (2013).
27. A. Singla *et al.*, *Nat. Commun.* **10**, 4271 (2019).
28. M. J. Kim, H. Jeong, D. Krainc, *Hum. Mol. Genet.* **31**, 2424–2437 (2022).
29. D. Schnabel, M. Schröder, K. Sandhoff, *FEBS Lett.* **284**, 57–59 (1991).
30. C. Valdez, D. Ysselstein, T. J. Young, J. Zheng, D. Krainc, *Hum. Mol. Genet.* **29**, 716–726 (2020).
31. M. Abu-Remaileh *et al.*, *Science* **358**, 807–813 (2017).
32. W. Peng, L. F. Schröder, P. Song, Y. C. Wong, D. Krainc, *Sci. Adv.* **9**, eadh3347 (2023).
33. A. E. Arrant *et al.*, *Acta Neuropathol. Commun.* **7**, 218 (2019).
34. T. Logan *et al.*, *Cell* **187**, 1565–1566 (2024).
35. X. Zhou *et al.*, *PLOS ONE* **14**, e0212382 (2019).
36. C. J. Holler, G. Taylor, Q. Deng, T. Kukar, *eNeuro* **4**, ENEURO.0100-0117.2017 (2017).
37. S. Mohan *et al.*, *Mol. Neurodegener.* **16**, 51 (2021).
38. G. Boncompain *et al.*, *Nat. Methods* **9**, 493–498 (2012).
39. J. Ecard *et al.*, *Mol. Biol. Cell* **35**, ar42 (2024).

40. R. Kalluri, V. S. LeBleu, *Science* **367**, eaau6977 (2020).
41. D. J. Boesch *et al*., *Nat. Struct. Mol. Biol.* **31**, 910–924 (2024).
42. S. Laulumaa, E. P. Kumpula, J. T. Huiskonen, M. Varjosalo, *Nat. Struct. Mol. Biol.* **31**, 925–938 (2024).
43. J. L. Burkhead, C. T. Morgan, U. Shinde, G. Haddock, S. Lutsenko, *J. Biol. Chem.* **284**, 696–707 (2009).
44. M. D. Healy *et al*., *eLife* **7**, e35898 (2018).
45. A. Fedoseienko *et al*., *Circ. Res.* **122**, 1648–1660 (2018).
46. A. Singla *et al*., *Dis. Model. Mech.* **14**, dmm045963 (2021).
47. C. G. Campion *et al*., *Cell Rep.* **24**, 670–684.e7 (2018).
48. H. Li *et al*., *J. Cell Biol.* **211**, 605–617 (2015).
49. V. J. Butler *et al*., *J. Mol. Biol.* **431**, 1038–1047 (2019).
50. C. Valdez *et al*., *Hum. Mol. Genet.* **26**, 4861–4872 (2017).
51. X. Zhou *et al*., *Acta Neuropathol.* **134**, 151–153 (2017).
52. S. Boland *et al*., *Nat. Commun.* **13**, 5924 (2022).
53. M. Reich *et al*., *Sci. Transl. Med.* **16**, eadj7308 (2024).
54. A. Reifschneider *et al*., *EMBO J.* **41**, e109108 (2022).
55. J. E. Hunter, J. Leslie, N. D. Perkins, *Br. J. Cancer* **114**, 1–6 (2016).
56. S. Bandres-Ciga *et al*., *Acta Neuropathol.* **142**, 223–224 (2021).
57. M. B. Makarious *et al*., *Brain* **146**, 4622–4632 (2023).
58. M. A. Nalls *et al*., *Lancet Neurol.* **18**, 1091–1102 (2019).
59. B. I. Bustos, bibb/Burden-analysis-of-rare-predicted-loss-of-function-variants-in-COMMD-related-genes-for-PD: v1.0, Zenodo (2025); https://doi.org/10.5281/zenodo.14798968.

ACKNOWLEDGMENTS

This study used genetic data from PD patients and healthy controls from the UK Biobank Resource under application no. 78210 and the Accelerating Medicines Partnership (AMP) program for Parkinson's disease (see acknowledgments in the supplementary materials). We thank Northwestern's Robert H. Lurie Comprehensive Cancer Center for the use of the Flow Cytometry Core Facility, supported by NCI P30 CA060553; the NUSeq Core Facility and Skin Biology & Diseases Resource-Based Center, supported by P30AR075049; and NU Center for Advanced Microscopy, supported by NCI P30 CA060553. We thank D. Dickson for providing human postmortem samples. **Funding:** This work was supported by National Institutes of Health grants R37 NS096241 and R35 NS122257 (D.K.). **Author contributions:** G.M., N.S., and D.K. conceptualized the study. G.M. and N.S. performed all experiments, with the exception of the genetic analysis, which was performed by B.I.B. and N.E.M. S.J.L. provided access to the genetic data. G.M., N.S., and B.I.B. analyzed data and prepared figures. G.M., N.S., B.I.B., and D.K. wrote the manuscript, which was edited and approved by all authors. D.K. provided project supervision and funding. **Competing interests:** D.K. is the founder and scientific advisory board chair of Vanqua Bio and serves as the scientific adviser to The Silverstein Foundation, Neuro.VC, and OrbiMed. The other authors declare that they have no competing interests. **Data and materials availability:** Whole-genome and exome sequencing data from PD patients and controls are available from AMP-PD and UK Biobank under a material transfer agreement (MTA). New materials generated in this study, including plasmids and cell lines, are available upon completion of an MTA. All inquiries and requests should be made to the corresponding author. All data necessary to support this paper's conclusions are available in the supplementary materials. This paper reports original code used to perform the burden analysis of rare predicted LOF variants in COMMD related genes, available at Gitbhub (https://github.com/bibb/COMMD-LOF-burden-in-PD) and Zenodo (*59*). Uncropped western blots corresponding to main and supplemental figures are included as part of the supplementary materials. CellProfiler pipelines, Fiji macros, and Python scripts used in image analysis are available as resource files.

SUPPLEMENTARY MATERIALS

science.org/doi/10.1126/science.adq6650
Materials and Methods
Supplementary Text
Figs. S1 to S9
Tables S1 to S4
References (*60*–*72*)
MDAR Reproducibility Checklist
Data S1 to S10

Submitted 24 May 2024; resubmitted 2 December 2024
Accepted 12 February 2025
10.1126/science.adq6650